INTERNAL WAVE DISSIPATION IN A NON-GARRETT-MUNK OCEAN

L. Padman[1], T.M. Dillon[1], H.W. Wijesekera[1], M.D. Levine[1], C.A. Paulson[1], and R. Pinkel[2]

[1]College of Oceanography, Oregon State University, Corvallis, OR 97331-5503.
[2]Scripps Inst. of Oceanography, La Jolla, CA 92093.

ABSTRACT

Recent work by M.C. Gregg has suggested that the dissipation rate of turbulent kinetic energy in the oceanic thermocline may be closely related to the internal wave shear variance measured at 10 m vertical scales. If this relationship holds, it significantly decreases the experimental effort required to estimate eddy viscosities and diffusivities. However, as Gregg has noted, the diffusivities associated with his model in a Garrett-Munk (GM) canonical wave field are quite small, and it therefore appears that mixing driven by internal waves may only be important where the mean energy level is substantially above GM. In this paper we explore the relationship between internal waves and microscale dissipation from a region of energetic mixing, near the Yermak Plateau in the Arctic Ocean. The dissipation rate is an order of magnitude above that predicted by Gregg's model, and we shall discuss several aspects of the local internal wave field which may contribute to this result. We also suggest one way in which Gregg's model might be modified to account for this new data set.

INTRODUCTION

The recent paper by Gregg (1989) (hereinafter G89), which suggested a close relationship between internal wave (IW) shear and dissipation rate, ϵ, has prompted a number of studies aimed either at (a) applying his results to other appropriate data sets, or (b) searching for locations in which the scaling model does not work. As Gregg himself has indicated (pers. comm., 1990), anomalous environments may be regions of large diapycnal transport of both momentum and scalars, perhaps dominating the basin-averaged diapycnal fluxes. It is therefore necessary to

determine why these regions differ from the cases studied in G89, and whether a predictive model, based on observed IW field properties, can be found for these regions. G89 noted that the diffusivities implied by the model applied to a GM wave field at the canonical energy density level are small, and may therefore not be relevant to the dynamics of the mid-ocean thermocline, except perhaps on time scales of decades or longer. Apparently then, the places to look for vertical mixing rates which are sufficiently large to be dynamically important are regions where the IW energy density is substantially higher than the canonical value. However, as the present analysis will show, regions where the energy density is not necessarily abnormally large, but the wave field deviates in other ways from the GM assumptions, can also be regions of large diapycnal transports.

One of the aims of Gregg's study was to find ways to reduce the field effort involved in estimating ϵ. One possibility, which he explored, was to use Expendable Current Profilers (XCPs) to determine the shear at 10 m vertical scales. For the data sets which he considered, shear variance was a good indicator of ϵ in some averaged sense. However, this method still requires that the experimentalist be present to launch the XCPs, and the questions of sampling bias in ϵ estimates due to small sample size (Baker and Gibson, 1987) still remain. In an ideal world, one would obtain estimates through all types of events which might contribute to ϵ within the time and space intervals of interest. For example, if ϵ could be linked to some basic variables which are obtainable from long-term moorings (*e.g.* IW energy density, and buoyancy frequency, N), then ϵ could be "monitored" throughout the life of the mooring. Unfortunately, as we shall show below, a model based simply on energy and N doesn't work well in some environments where mixing is important. However, there may be higher order IW statistics which could be measured, and used to improve models. The requirements for models are not as strict as they might seem at first, since even a factor of two error in a model prediction might be much less than the errors involved in extrapolating the results of a short-duration microstructure or XCP program.

The data set which we shall use to explore this topic was obtained from the Oceanography ("O") Camp, deployed on the pack ice in March-April 1989 during the Coordinated Eastern Arctic Experiment (CEAREX). A background paper which fully describes the program and the data is in press (Padman and Dillon, 1991; hereinafter PD91), however a short review is provided in the following section of the current paper. We then review some of the anomalous characteristics of the O Camp IW climate, followed by a discussion of the implications for predictive modelling of ϵ in this environment. There are two seemingly dichotomous

aims to this study: first, we wish to show how the observed wave field is inconsistent with the assumptions of existing wave/dissipation models; and second, we wish to indicate that some modelling success can be retained despite these inconsistencies. Hopefully, however, the two approaches are actually complementary, even if the empirical modeling is primarily a short-term effort awaiting the construction of more versatile IW dissipation models.

THE CEAREX PROGRAM

CEAREX was a multi-investigator Arctic oceanographic experiment conducted from several platforms, including the O Camp from which the data discussed in this paper were obtained. Apart from direct microstructure measurements, data from O Camp include Acoustic Doppler Current Profiler (ADCP) measurements in the upper several hundred meters, and densely sampled CTD data, as well as water depth and meteorological information. A schematic of the various programs at O Camp is shown in Fig. 1. The drift track (Fig. 2) was determined from ap-

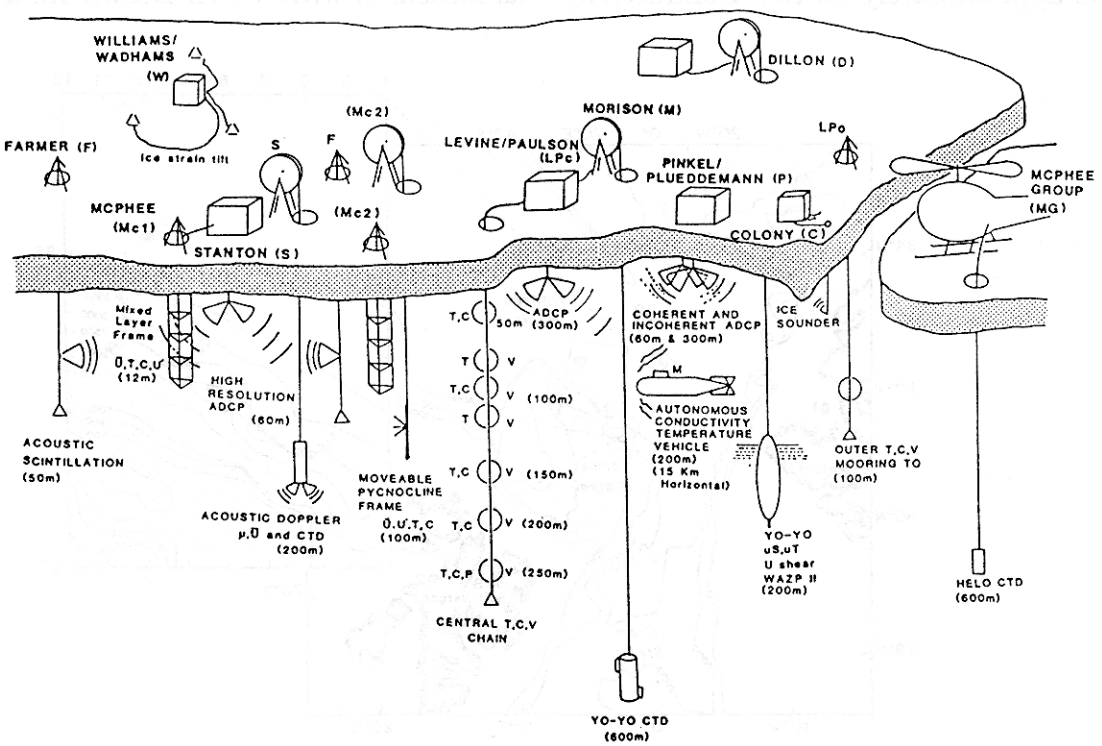

Fig. 1. Schematic of CEAREX O Camp, showing the principal sampling programs.

proximately hourly satellite fixes, then smoothed with the complex demodulation algorithm described by McPhee (1988). This algorithm assumes that the ice motion consists solely of tidal and inertial oscillations, and low-frequency drift.

Approximately 1500 microstructure profiles were made with the Rapid-Sampling Vertical Profiler (RSVP) (Caldwell, *et al.*, 1985; Padman and Dillon, 1987) from March 31 to April 25, 1989. Data were obtained between the surface and a typical maximum depth of 340 m, and the cycling time between profiles was usually 15–20 minutes. The RSVP (Fig. 3) is a tethered, freefall profiler about 1.3 m long, equipped with sensors for measuring pressure, P, orthogonal microscale velocity shears, $u_z(= \partial u/\partial z)$ and $v_z(= \partial v/\partial z)$, temperature, T, and conductivity, C. The average fall rate is about 0.7 m s^{-1}, constrained by a drag element consisting of an annular brush near the rear of the probe during descent, but able to slide towards the RSVP's nose for improved retrieval dynamics. A profile to 340 m takes about 8 minutes. The raw data sampling rate during CEAREX was 256 Hz for all channels. Microscale temperature was measured with a Thermometrics FP07 thermistor (T_1) projecting forward from the probe nose assembly. Gregg and Meagher (1980) measured a 3-dB attenuation point for similar thermistors to be approximately 15 Hz. Conductivity was measured with a Neil Brown Instru-

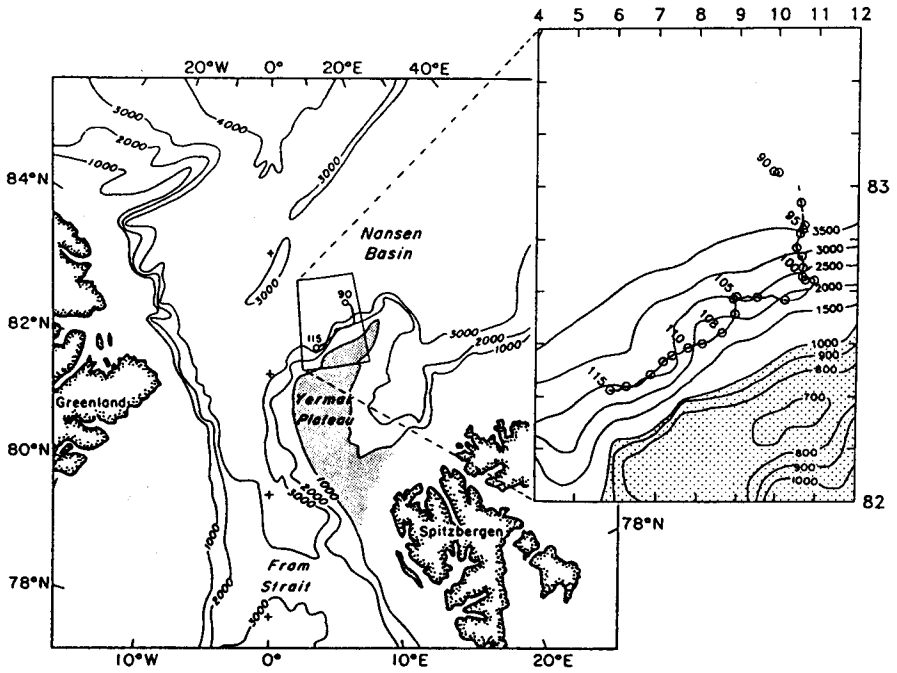

Fig. 2. Drift track of the CEAREX O Camp. Depth contours are in meters. Symbols are given once daily, and are marked in day-of-year (1989).

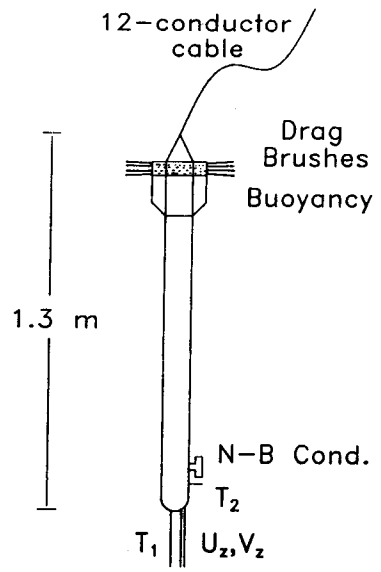

Fig. 3. Schematic of the Rapid-Sampling Vertical Profiler. Sensors are thermistors (T_1 and T_2), conductivity cell (*N-B Cond.*), pressure transducer (P), and airfoil shear probes (U_z and V_z).

ment Systems (NBIS) conductivity cell ($N - B\ Cond.$) mounted on the side of the probe, 0.15 m above the probe tip. For salinity determination a second FP07 thermistor (T_2) was mounted adjacent to the conductivity sensor. The NBIS cell has a response length of O(0.1) m (Gregg *et al.*, 1982), so that at the nominal fall rate the time constant of the conductivity cell is 0.14 s. Post-analysis of the conductivity data indicated a small, time-varying calibration offset voltage: conductivities have therefore been corrected by comparison with CTD data, provided by J. Morison. Vertically averaged salinity, S, was determined from similarly filtered T and C: the effective resolution for S and density, σ_t, is about 0.2 m. Least significant bit (*lsb*) resolutions of the raw 16-bit records are about 1.5×10^{-4}°C in temperature, and 1.5×10^{-5} S m^{-1} in conductivity. Typical *rms* noises, based on measurements deep within non-turbulent surface mixed layers, are comparable to the *lsb* resolutions.

Velocity microstructure was measured with two orthogonally mounted airfoil shear sensors (U_z, V_z) on the RSVP's nose. These probes (Osborn and Crawford, 1980) have a spatial resolution of about 0.02 m, sufficient to resolve most of the "universal", or Kolmogorov, shear spectrum for typical oceanic dissipation rates. Estimates of ϵ were made for approximately 1.4 m depth intervals (2 s of data)

by integrating the velocity shear spectra in the wavenumber range of 2 to 20 cpm. Assuming isotropy of velocity fluctuations in this wavenumber band,

$$\epsilon = \frac{15}{2}\nu\left\langle\frac{u_z^2 + v_z^2}{2}\right\rangle \tag{1}$$

where ν is the kinematic viscosity of seawater, about 1.8×10^{-6} m^2 s^{-1} at these low temperatures, and $\langle\ \rangle$ denotes vertical averaging. The noise level based on measured microscale shears in the quietest regions appears to be about 10^{-9} W kg^{-1}, substantially higher than during the Arctic Internal Wave Experiment, AIWEX, (Padman and Dillon, 1987). We believe that this is due to a change in the dynamics of the RSVP, which in CEAREX was an air–filled, pressure–sealed case compared with an oil–filled instrument in AIWEX. The probable result of the latter change, which was compensated for by a reduction in the number and size of drag and buoyancy elements near the instrument's tail, is an increase in motion near the instrumented nose. However, ϵ in energetic mixing patches was 10^3 times greater than the noise level, so that the mixing processes which contribute most to the time–averaged evolution of the large–scale hydrographic fields were well resolved. The noise level was lowest in regions where the thermal gradients were smallest, notably in a warm, almost isothermal Atlantic Layer slab which was sampled at the end of the experiment. This suggests that the shear probes' thermal response, discussed by Osborn and Crawford (1980), may also contribute to setting the noise level on ϵ measurements.

An *upper* limit on fully resolved shear spectra is determined by the finite response length scale of the airfoil shear probes. The universal shear spectrum contains energy at all scales larger than the Kolmogorov microscale,

$$l_k = 2\pi(\nu^3/\epsilon)^{1/4} \tag{2}$$

although the spectral peak occurs at wavelengths of about $10l_k$. For $\epsilon = 1 \times 10^{-6}$ m^{2}s^{-3}, l_k is about 0.01 m, and the peak spectral density lies at wavelengths of about 0.1 m. Some correction can be made for the frequency response of the shear probes, however in all the data discussed in this paper the correction to ϵ was less than 20%, which is smaller than the potential calibration errors on the probes themselves. Therefore, in this paper, no spectral corrections have been applied.

The complete transect of ϵ averaged over 4 hours and 10 vertical meters is shown in Fig. 4. Time, t, is given throughout this paper in decimal day-of-year (UTC), where t=1.0 is 00:00 h on January 1,1989. High dissipation rates near the sur-

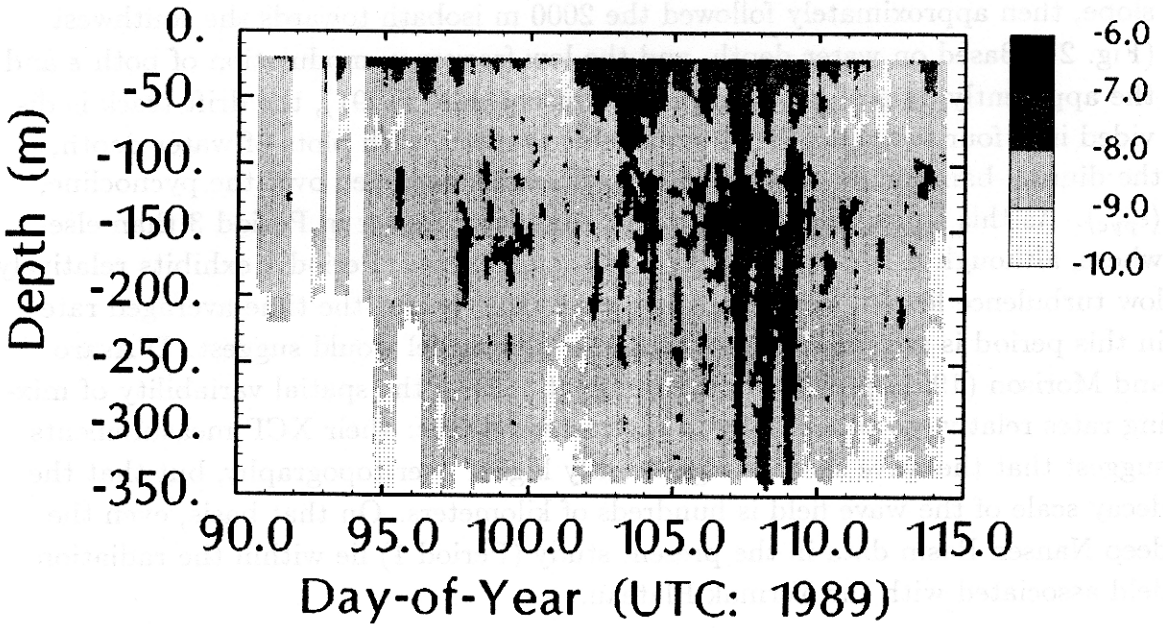

Fig. 4. Transect of dissipation rate, $\log_{10}(\epsilon)$, throughout the O Camp drift. Data have been averaged over 4 hours and 10 vertical meters.

face between t=101 and 110 are related to high surface stresses resulting from enhanced diurnal tidal currents which are a well-documented phenomenon in this region (Hunkins, 1986; PD91). Of more interest to the present paper are the large, quasi-diurnal bursts of high dissipation in the pycnocline (below about 100 m), which also occur during this period of strong diurnal tides. We shall discuss the possible causes of these bursts after reviewing the IW field which is assumed to initiate the mixing.

THE INTERNAL WAVE FIELD

The O Camp phase of CEAREX was exceptionally well set up for the study of the IW field (see Fig. 1). Simultaneous measurements were made of the hydrographic and current variability throughout the upper several hundred meters of the water column, encompassing almost all of the density stratification. A horizontal array provided information on the propagation direction of specific wave packets, while unique measurements of ice tilt and strain related to the passage of wave packets were also collected (P. Czipott, pers. comm., 1990). The ice camp drifted southward from the deep water of the Nansen Basin, up the plateau

slope, then approximately followed the 2000 m isobath towards the southwest (Fig. 2). Based on water depth, and the low frequency modulation of both ϵ and the apparently dynamically significant diurnal tide (PD91), the drift track is divided into four sections. Fig. 5 shows this division, with plots of water depth, the diurnal-band major axis current speed, and ϵ averaged over the pycnocline, $\langle \epsilon_{pyc} \rangle$. As this figure shows, $\langle \epsilon_{pyc} \rangle$ is substantially higher in Period 3 than elsewhere, although it is dominated by a few large events. Period 1 exhibits relatively low turbulence levels. However, as we shall show below, the time-averaged rate in this period is still much larger than the G89 model would suggest. D'Asaro and Morison (1991) provide an independent view of the spatial variability of mixing rates relative to topography in the eastern Arctic: their XCP measurements suggest that the wave shear is significantly higher over topography, but that the decay scale of the wave field is hundreds of kilometers. On that basis, even the deep Nansen Basin data in the present study (Period 1) lie within the radiation field associated with the Yermak Plateau.

The mean profiles of buoyancy frequency, N, dissipation rate, ϵ, and wave field energy density, E_{meas}, for the entire experiment are shown in Fig. 6. These profiles were made by first mapping the velocity field from the ADCPs to approximate isopycnal coordinates in order to reduce the vertical "smearing" by the large-amplitude diurnal oscillations. The resultant along-isopycnal averages are then plotted as a function of mean isopycnal depth. This "semi-Lagrangian" approach will be used throughout this paper. The energy density, E_{meas}, was calculated as

$$E_{meas} = \frac{1}{2}\left[\langle \eta^2 \rangle N^2 + \langle U^2 \rangle + \langle V^2 \rangle\right] \tag{3}$$

where

$$\langle \eta^2 \rangle = \int_f^{\omega_{nyq}} \Phi_\eta(\omega) d\omega \tag{4}$$

and

$$\langle U^2,\ V^2 \rangle = \int_f^N \left[\Phi_u(\omega),\ \Phi_v(\omega)\right] d\omega \tag{5}$$

$\Phi_\eta(\omega)$ is the power spectral density of RSVP isopycnal displacements, $\Phi_u(\omega)$, $\Phi_v(\omega)$ are the power spectral densities of orthogonal velocity components, and f and ω_{nyq} are the local inertial frequency ($\approx 1.45 \times 10^{-4}$ s^{-1}) and the Nyquist frequency ($\omega_{nyq} \approx$ 1 cycle per hour for RSVP data) respectively. The vertical velocity variance is negligible compared with the horizontal components, and is therefore ignored in determining E_{meas}.

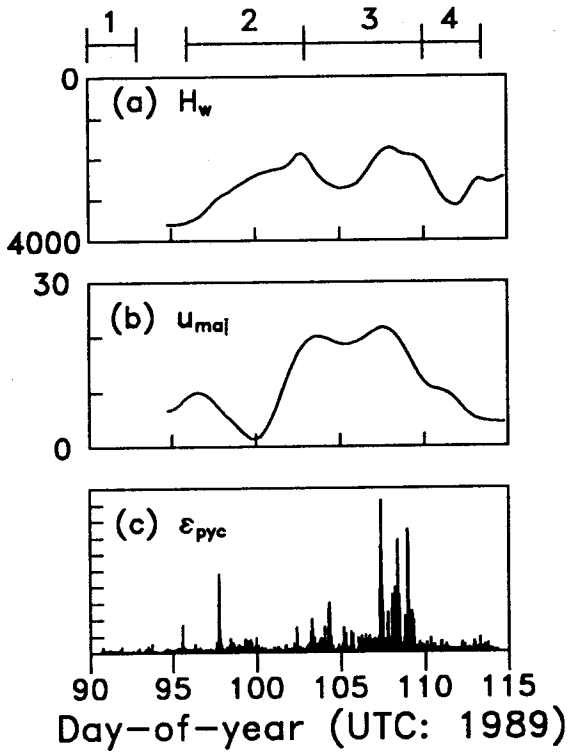

Fig. 5. (a) water depth (m), (b) diurnal-band major axis current (cm s^{-1}), and (c) dissipation rate (m^2s^{-3}) averaged through the pycnocline. Horizontal bars indicate the division of the experiment into 4 periods.

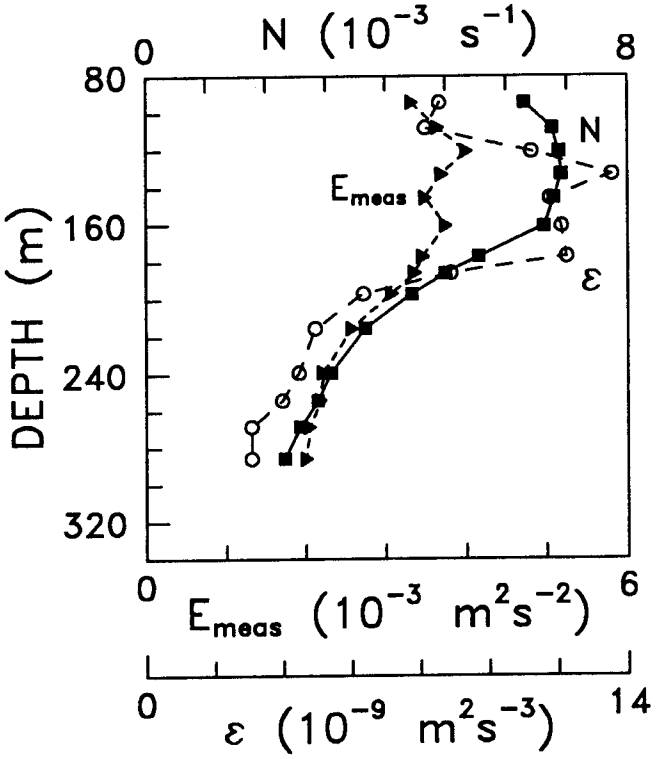

Fig. 6. Mean profiles of buoyancy frequency (N), dissipation rate (ϵ), and internal wave energy density (E_{meas}), for the period $96 < t < 114$.

The highest dissipation rates and energy densities occur in the upper, strongly stratified pycnocline, with a decay to lower values in the less strongly stratified region associated with the Atlantic Water core near 250 m. Based on these profiles, we consider the pycnocline to consist of 3 regions; the strongly stratified upper pycnocline, $100 < z < 170$ m; a transition zone, $170 < z < 220$ m; and the lower pycnocline, $220 < z < 270$ m. The wave field experienced by each region in each period varies widely, with commensurate changes in the mean dissipation rates.

Table 1 presents some basic characteristics of the IW field for each of the time and depth ranges. Buoyancy frequency changes by a factor of about two from the upper (U) to lower (L) pycnocline, however the mean profile of $N(z)$ changes very little from one period to the next. Except for the first period, however, the

energy density scaled by the N-scaled GM level varies significantly with depth, indicating that WKB scaling of the wave field is not valid. The measured dissipation rate varies from about 1 $\times 10^{-9}$ to 20 $\times 10^{-9}$m^{2}s^{-3}, however, values of less than 2 $\times 10^{-9}$m^{2}s^{-3} may be seriously biased by noise (see the description of the RSVP, above). The *rms* internal wave band strain, $\lambda^{IW}_{10,rms}$, is a measure of the IW-induced variability of N, and is discussed in more detail below.

Table 1: Mean properties of the internal wave field and dissipation rates for the four time periods shown in Fig. 5, and for mean isopycnal depth ranges of 100–170 m (U), 170–220 m (T), and 220–270 m (L). Tabulated parameters are: buoyancy frequency, $\langle N \rangle$ ($\times 10^{-3}$ s^{-1}); mean energy density, $\langle E_{meas} \rangle$ ($\times 10^{-3}$ m^{2}s^{-2}); mean energy density scaled by N-scaled Garrett-Munk energy density, E_o; *rms* internal-wave-band strain evaluated over 10-m mean isopycnal separation, $\lambda^{IW}_{10,rms}$; equivalent number of vertical modes, j_*; measured mean dissipation rate, ϵ_{meas} ($\times 10^{-9}$m^{2}s^{-3}); and decay time scale, $\tau = \langle E_{meas} \rangle / \epsilon_{meas}$ (days).

Period	Depth range	$\langle N \rangle$	$\langle E_{meas} \rangle$	$\langle E_{meas} \rangle / E_o$	$\lambda^{IW}_{10,rms}$	j_*	ϵ_{meas}	τ
1	U	6.7	1.12	0.30	–	6	2.0	6
	T	4.8	0.66	0.25	–	6	1.2	6
	L	2.9	0.41	0.26	–	6	1.6	3
2	U	6.7	2.23	0.60	0.37	7	7	4
	T	4.8	2.66	1.01	0.40	7	4	8
	L	2.9	2.24	1.40	0.48	7	2.0	13
3	U	6.7	5.79	1.56	0.43	4	20	3
	T	4.8	4.09	1.55	0.51	4	16	3
	L	2.9	3.95	2.48	0.53	4	9	5
4	U	6.7	4.16	1.13	0.36	5	6	8
	T	4.8	3.33	1.26	0.39	5	4	10
	L	2.9	3.54	2.22	0.32	5	2.0	20
GM		5.2	2.9	1.0	0.27	3	–	–

A particularly interesting aspect of data from the Arctic Ocean is the close proximity of the semi-diurnal tidal lines to the inertial frequency, f. For example, at 83° N, the frequency of the M_2 tidal line is about $0.97f$. Therefore, while the M_2 tide is formally a subinertial oscillation, the addition of relatively little negative

relative vorticity, $-|\zeta|$, to the planetary vorticity can result in the M_2 baroclinic tide becoming a free wave (*i.e.* $\omega > f - |\zeta/2|$). This effect is discussed in more detail in D'Asaro and Morison (1991). Perhaps more importantly, it becomes difficult or impossible to determine the free wave contribution from a near-inertial spectral peak, especially when measured from a non-stationary ice camp.

Fig. 7 shows frequency spectra for several relevant variables during the ice drift. These spectra are taken along an isopycnal with a mean depth near 150 m, near the ϵ peak, for the period $97.0 < t < 113.0$. The velocity spectrum is dominated by diurnal energy, with a secondary peak, as expected, near the inertial frequency. The cartesian coordinate shear spectrum shows that the diurnal tide is almost entirely barotropic, so that the near-inertial peak dominates. When the *magnitude* of the shear vector is analyzed (Fig. 7d) the dominant peak is again near-inertial, consistent with a shear vector that rotates with time rather than showing appreciable magnitude changes. Other spectra show the principal frequencies of variability in N, strain, and ϵ, and will be discussed further below. However, for the moment it is worth noting that the dominant time scales for variability of ϵ are diurnal and approximately 6 hours, the latter *not* corresponding to significant peaks in any of the obvious forcing functions.

With this degree of wave field variability in mind, we now consider higher order statistics of the displacement field, to see if there might be some obvious reason for the failure of the G89 model in this environment. One possible candidate is the effective vertical wavenumber bandwidth, β_*, which appears in the McComas and Müller (1981) and Henyey *et al* (1986) models (Eqs. 9 and 10, below). In practice, because β_* is expected to be a function of N, we consider instead the variability in the "equivalent number of vertical modes", $j_* = bN_o\beta_*/\pi N$, where N_o is a canonical buoyancy frequency ($0.0052\ \mathrm{s}^{-1}$), and b is the scale depth of the thermocline (1300 m). A typical mid-latitude value is $j_* = 3$.

Desaubies and Smith (1982) used an analytical approximation (Desaubies and Gregg, 1981) to the GM spectrum to show that shear variance was simply related to kinetic energy density by

$$\langle U_z^2 \rangle = \beta_* \beta_c \langle U^2 \rangle \tag{6}$$

where β_c is the cutoff wavenumber in the IW field, which Gargett *et al* (1981) suggested was constant at about $0.6\ \mathrm{m}^{-1}$. Desaubies and Smith argued that the statistics of mixing in a GM IW field are dependent only on the *rms* strain, λ_{rms}, where

$$\lambda_{rms}^2 = \langle (\partial\eta/\partial z)^2 \rangle \tag{7}$$

and η is an isopycnal displacement from its mean position. Desaubies and Smith speculated that the (at the time) apparent constancy of λ_{rms} in the open ocean

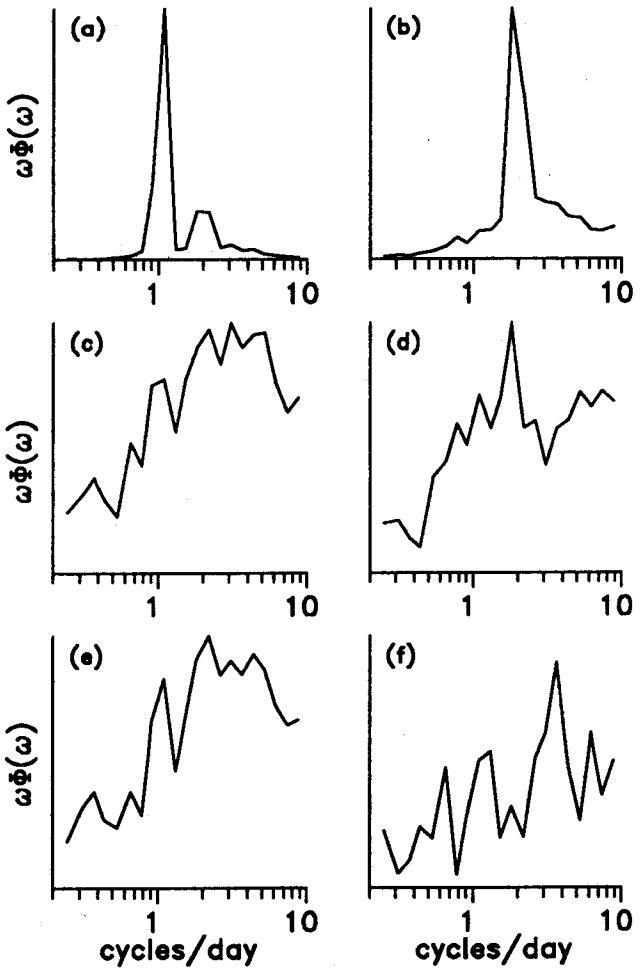

Fig. 7. Area-preserving frequency spectra of (a) currents, (b) shear components, (c) buoyancy frequency, (d) shear *magnitude*, (e) strain, and (f) pycnocline-averaged dissipation rate.

indicated that the ϵ was related to the saturation of the IW field at a level where breaking instabilities rapidly drained energy from the waves. Their numerical simulations indicated that ϵ was extremely sensitive to λ_{rms}, as well as being strongly influenced by the addition of near-inertial shear to the GM level. The overall result was a model which, while producing plausible diffusivities, was too sensitive to be usefully applied to field measurements. Nevertheless, the concept that strain might be an important parameter to monitor is valuable, and we shall show below that the CEAREX data set exhibits strain rates which are much larger than are typical in the mid-ocean thermocline.

As with other analyses in this paper, strain is measured in isopycnal-following coordinates. We have traced 100 isopycnals, having a mean separation of Δz = 1.7 m, and spanning the range of 100 to 270 m mean isopycnal depth, through the RSVP data set between t=96.0 and t=114.0. The original profiles were pre-filtered to 0.7 m resolution in order to minimize the impact of salinity spiking. A local value of strain is estimated as

$$\lambda_\delta = \frac{\eta(\overline{z_i}) - \eta(\overline{z_i} + \delta)}{\delta} \tag{8}$$

where δ is the mean separation of isopycnal pairs between which strain is being estimated. For consistency with G89 we will generally use λ_{10}. This choice of δ = 10 m also reduces the noise associated with interpolation from the equi-spaced (in depth) original profiles. The time series for finite-differenced strain between each isopycnal pair is then filtered to remove variability at frequencies below $0.8f$, most of which is due to compression of isopycnals as the barotropic diurnal tidal currents flow across the plateau slope. The *rms* strain is then simply the square root of the variance of λ_δ evaluated throughout the time and depth ranges of interest. The value of λ_{rms}, based on a 10 m mean isopycnal separation and after filtering, is denoted $\lambda^{IW}_{10,rms}$. Values of $\lambda^{IW}_{10,rms}$ are included in Table 1 for the three depth ranges and the latter three time periods (there were insufficient profiles in the first period to allow reliable isopycnal tracking). However, note that the true *rms* strain (Eq. 7) is very sensitive to the cutoff wavenumber of the wave field: the choice of β_c=0.63 m^{-1} is based on Gargett *et al* (1981), rather than being substantiated by the present data.

The values of $\lambda^{IW}_{10,rms}$ in Table 1 are all much larger than the 10 m *rms* strain expected for a GM ocean with j_* = 3. The dissipation rate which the Desaubies and Smith model therefore predicts is orders of magnitude higher than in a canonical ocean. There is a trend in periods 2 and 3 towards higher strain rates with decreasing N. Desaubies and Smith (1982) noted that, with a WKB-scaled wave field, $\lambda_{\delta,rms}$ should be independent of depth (and N). As we found with the N-dependence of energy density, this result suggests that WKB scaling is inappropriate to the present environment.

Another aspect of the wave field which deviates markedly from the GM76 assumptions is the presence of intermittent, but large-amplitude, wave packets. Fig. 8 shows the passage of one such packet as measured from a thermistor moored at 150 m. As suggested by PD91, there is some evidence that the mixing rates are correlated with these wave packets, which are in turn weakly correlated with the observed amplitude of the diurnal currents. One hypothesis is therefore that these waves are generated somewhere over the Plateau by the cross-shelf flow of the diurnal tide, then propagate towards deep water. While the generation mechanism itself is unclear, this scenario is supported by D'Asaro and

Morison's (1991) estimates of the decay scale of shear variance away from topography, and our own observations of the spatial dependence of ϵ from O Camp. Furthermore, both ice tilt measurements (P. Czipott, pers. comm., 1990) and estimates of phase propagation from the horizontal array of T, C and current sensors at O Camp indicate a cross-slope phase propagation towards deeper water. Coherent wave packets such as this violate the GM76 assumptions both of random phase between different waves, and isotropy. It is not clear how to take such packets into account, other than to re-run the HWF eikonal model with such waves included, however there is a strong possibility that such anomalous waves contribute substantially to the observed mean mixing rates.

The anisotropic nature of these near-N waves is also apparent in plots of the vertical coherence of semi-Lagrangian alongslope and cross-slope currents as a function of frequency (Fig. 9). While there is no anisotropy apparent in energy density when smoothed over a number of days, the cross-slope current is much more vertically coherent than the alongslope current. Our view is that this relatively high coherence arises from the passage of these near-N wave packets, even though the contribution of the packets to the time-averaged near-N energy density is small.

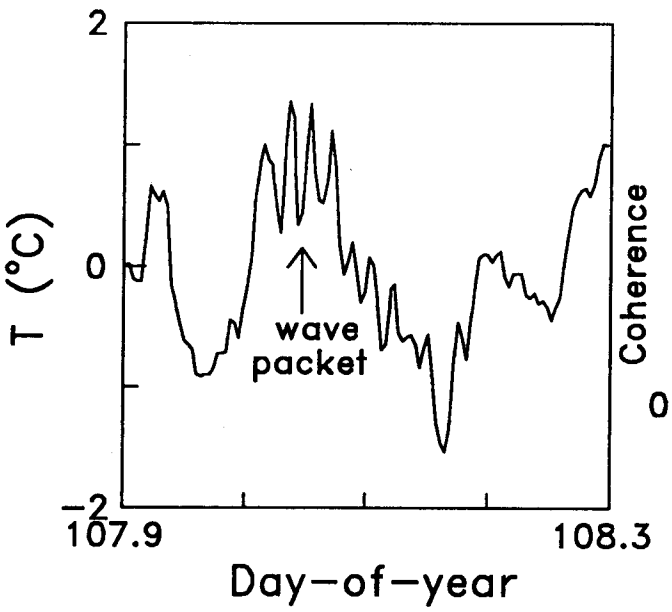

Fig. 8. Temperature at 150 m during the passage of a high-frequency wave packet past O Camp.

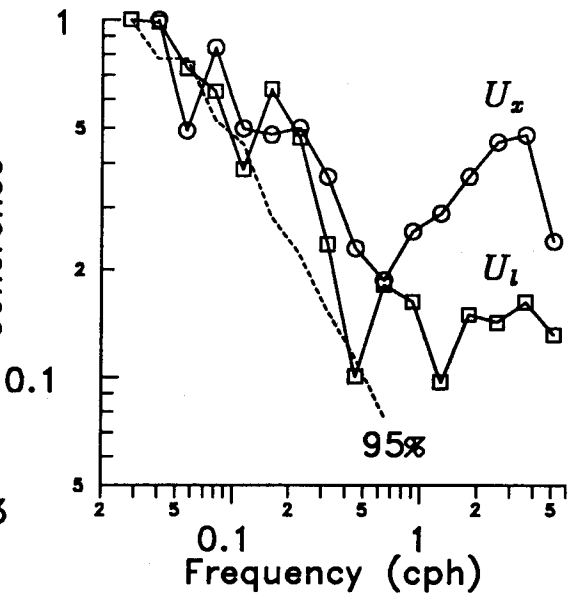

Fig. 9. Coherence, over 20 vertical meters, for cross-slope (U_x) and alongslope (U_l) currents in the pycnocline during the most energetic mixing period $103<t<110$. Dashed line indicates the 95% confidence level.

Finally, we are left not fully understanding the cause of the 6-hour peak in the area-preserving spectrum of ϵ (Fig. 7f). We have seen (Figs. 7c and 7d) that no such peaks exist in the density gradient or shear magnitude spectra. A cross-spectrum of shear *magnitude* and N shows no coherence at this frequency. However, a small but significant coherence is found near 4 cycles/day in the cross-spectrum of cross-slope shear with N, and similarly with along-slope shear and N. We postulate that the high frequency wave packets are in some way related to the 6-hour waves, and that the enhanced mixing at this periodicity is related to low Richardson number events which occur on time scales which are too short to be resolved by the present CTD data. Fig. 10 shows the band-passed (1/7 to 1/5 hour) isopycnal displacements plotted as a function of mean isopycnal depth, for the 5-day period when mixing was most energetic. There is evidence of both downward energy propagation (upward phase), particularly in the first 2 days, and upward energy propagation for $107 < t < 109.5$. The highest dissipation rates (Fig. 4) occur during the period of upward energy flux in this frequency band.

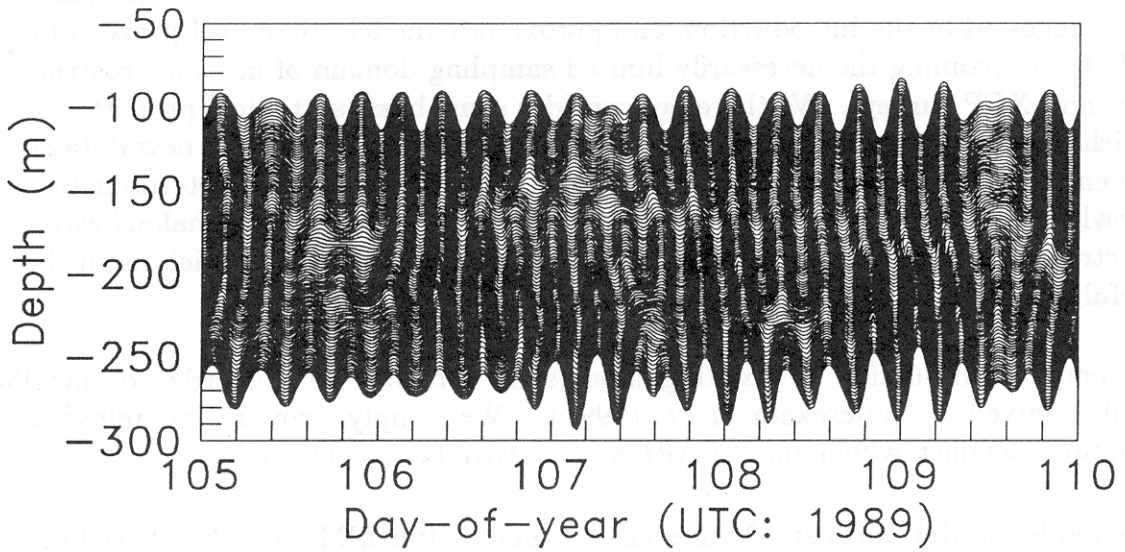

Fig. 10. Band-passed ($1/7 < \omega < 1/5$ cph) density field for the period $105 < t < 110$. For presentation, the mean density at each depth has been added to the band-passed signal.

Carrying this scenario further, we suspect that the 6-hour waves might be generated at the seabed as a higher harmonic of the cross-slope diurnal tidal current, propagate upwards into the main pycnocline, then create the near-N wave packets as a response to the rapidly increasing shear as the vertical wavelength is compressed by increasing N. This would be consistent with the highest values of ϵ being found *below* the depth of maximum N (see Fig. 6), since significant energy would presumably be lost from the upward-propagating waves in this region.

The proposed mechanism (above) is clearly highly speculative, and it is probable that it will remain so in the foreseeable future. The available bathymetry in this region is totally inadequate for an assessment of the bottom slope in any detail, while the buoyancy frequency profile of the deep ocean in this region is also inadequately sampled. It is therefore not possible to construct a robust model of wave reflection and propagation in this region. Nevertheless, we believe that all the data point towards a vertical anisotropy in the wave fluxes, at least within certain frequency bands, which again is a violation of the GM tenets.

DISSIPATION RATE MODELS

We have shown in the previous Section that the wave field during the CEAREX O Camp drift differs in many respects from the canonical GM wave field. It would not be surprising, therefore, if models based on the GM parameterization failed to adequately describe ϵ in such anomalous wave fields. Nevertheless, as was suggested in the Introduction, an approximate model might still prove valuable by overcoming the necessarily limited sampling domain of most microstructure and XCP surveys. We therefore consider some basic statistical properties which might allow existing models to be extended to cope with this new data set. We emphasize, however, that this effort does not imply increased deterministic knowledge of the processes involved in energy transfer through anomalous wave spectra. The aim is simply to look for a refined empirical model which might be useful while the wave field dynamics continue to be explored.

A complete discussion of existing models of ε related to properties of the IW field is given in Wijesekera *et al.* (1991). We simply provide the relevant equations against which the CEAREX data will be compared.

The model of McComas and Müller (1981) (hereinafter MM), which is based on weak resonant interactions between internal waves, is:

$$\epsilon_{MM} = \left(\frac{27\pi}{32\sqrt{10}} + 1\right) \pi^2 b^2 N^2 f j_*^2 E_{GM}^2 , \qquad (9)$$

where E_{GM} $(= E/b^2 N N_o)$ is the GM dimensionless energy.

The model of Henyey, Wright and Flatté (1986) (hereinafter HWF) is based on an eikonal approach in which the nonlinear interactions are dominated by scale-separated interactions, with no effect on the large-scale background field. HWF predict a mean value of ϵ in a GM ocean of

$$\epsilon_{HWF} = \left[\frac{1.67}{\pi}\right] f j_*^2 b^2 N^2 E_{GM}^2 \, cosh^{-1}\left[\frac{N}{f}\right] \qquad (10)$$

Note that the forms of ϵ_{MM} and ϵ_{HWF} are similar: as G89 noted, $\epsilon_{MM} \approx 7\epsilon_{HWF}$ for reasonable values of f and N.

Finally, the G89 model, expressed in terms of 10 m shear, S_{10}, is

$$\epsilon_{G89} = 7 \times 10^{-10} \frac{\langle N^2 \rangle}{N_0^2} \frac{\langle S_{10}^4 \rangle}{\langle S_{GM}^4 \rangle} \tag{11}$$

where $\langle S_{GM}^2 \rangle$ is the variance of shear at vertical scales greater than 10 m in the GM canonical, N-scaled ocean. If, as G89 assumed, the 10 m shear variance is simply related to the energy density by

$$\frac{S_{10}^2}{S_{GM}^2} = \frac{E_{IW}}{E_{GM}}, \tag{12}$$

where $E_{IW} = E_{meas}/b^2 N N_o$, then $\epsilon_{G89} \approx \epsilon_{HWF}$ for the mid-latitude data which he considered, provided GM canonical values of j_* (=3) and b (=1300 m), are used in calculating ϵ_{HWF}. G89 also investigated the f-dependence in the other models, but the test was inconclusive. The evaluation of S_{10}^2 from the O Camp ADCP data is difficult: Wijesekera *et al.* (1991) attempt to quantify the shear variance which is not resolved as a result of the vertical averaging scales for currents and finite-differencing to obtain shear; however the result is very sensitive to the choice of cutoff wavenumber, β_c, and the slope of the shear spectrum at the unresolved wavenumbers. For comparison with the measured dissipation rates, we therefore introduce an "energy-dependent" Gregg model, ϵ_E, based on (11) and (12):

$$\epsilon_E = 7 \times 10^{-10} \frac{\langle N^2 \rangle}{N_0^2} \frac{E_{IW}^2}{E_{GM}^2} \tag{13}$$

The essential difference between Gregg's scaling model and the MM and HWF models is that Gregg's model requires measurements of the velocity shear, while the MM and HWF models require estimates of the wave field energy density, E_{meas}, and the vertical wavenumber bandwidth, expressed as an equivalent number of vertical modes, j_*. Since energy density is relatively easily obtained from current meter moorings, the problem is therefore in estimating j_*. Gregg's assumption that j_*=3 is clearly not universally true: previous work in the Canada Basin (Levine, 1990; D'Asaro, pers. comm., 1990) indicate that $j_* \approx 30 - 60$ in that region. The Canada Basin is a site where E_{meas} is only about 10% of GM, but the shear variance associated with the greater number of equivalent modes is much closer to mid-latitude levels. We estimate j_* in the present data by calculating the correlation, r, between pairs of isopycnals with a mean separation of about 10 m. Then, for $\beta_c \gg \beta_*$, $\beta_* \approx -\ln(r)/\delta$: $\delta = 10$ m (from Desaubies and Smith (1982), Eq. 16). The value of j_* is then given by $bN_o\beta_*/\pi N$. The

measured vertical coherences indicate that $j_* \approx 6$ during CEAREX, although it actually varies from about 4 to 7 between periods (Table 1). The MM and HWF models therefore predict values of ϵ which are about 4 times greater than for $j_* = 3$. The f-scaling in those two models also implies dissipation rates which are a factor of two higher in the Arctic than at mid-latitudes.

It is not known yet why j_* in the Arctic is larger than in the deep, mid-latitude oceans. Nevertheless, if an experiment is somehow able to estimate j_*, then predictions of ϵ could be made based on both E and j_*. Table 2 shows how the three models compare with the measured averages for the same time and potential density ranges discussed above. In the mean, the energy-based, modified Gregg model underestimates ϵ_{meas} by about a factor of 6, although a factor of two improvement occurs if the prediction is f-scaled. MM overpredicts ϵ_{meas} by a factor of 3, while HWF underpredicts by a factor of 2.3. However, there is a large scatter in predictive ability for each model between different time and depth ranges.

Table 2: Measured mean dissipation rate, ϵ_{meas} ($\times 10^{-9} \mathrm{m^2 s^{-3}}$); and model predictions scaled by ϵ_{meas} for the time and depth ranges shown in Table 1.

Period	Depth range	ϵ_{meas}	ϵ^*_{MM}	ϵ^*_{HWF}	ϵ^*_E	ϵ^*_λ
1	U	2.0	0.55	0.07	0.06	–
	T	1.2	0.33	0.04	0.03	–
	L	1.6	0.09	0.01	0.01	–
2	U	7	2.0	0.29	0.06	0.21
	T	4	5.0	0.73	0.15	0.73
	L	2.0	7.0	1.0	0.21	2.1
3	U	20	1.55	0.22	0.14	0.90
	T	16	0.94	0.13	0.09	1.13
	L	9	1.56	0.22	0.14	2.11
4	U	6	4.17	0.60	0.25	0.77
	T	4	4.0	0.58	0.24	1.03
	L	2.0	9.0	1.3	0.53	1.05
Mean	–	–	3.02	0.43	0.16	1.02

The final column in Table 2 is an empirical prediction of dissipation rate, based on the assumption that the higher strain rates are indicative of higher shear and/or greater probability of instabilities occurring in the wave field. We assume that the strain-based predicted dissipation rate, ϵ_λ, is given by

$$\epsilon_\lambda = 7 \times 10^{-10} \frac{\langle N^2 \rangle}{N_0^2} \left(\frac{\lambda^{IW}_{10,rms}}{\lambda^{DS}_{10,rms}} \right)^4 \tag{14}$$

i.e. functionally similar to the G89 version (Eq. 11), with *rms* strain replacing shear. The 10-m strain in the GM canonical wave field, following Desaubies and Smith (1982) is $\lambda^{DS}_{10,rms} \approx 0.27$. The mean predictive ability of this empirical model is exceptionally good. We emphasize that there is little theoretical justification for this model, which is a hybrid of Gregg's scaling arguments and Desaubies and Smith's strain-based numerical simulations. In a GM wave field, shear is predominantly near-inertial, while the peak in the strain spectrum is shifted towards higher frequencies. In the present data set, the internal wave continuum, $\omega \gg f$, is amplified more than the near-inertial band near the plateau, so that the ratio of *rms* strain to *rms* shear is increased. Our results suggest that variability of N in the present data set will therefore be more important to the occurrence of the low Richardson number events (which we believe lead to turbulence) than in the mid-ocean thermocline, where variability of shear is most significant. Since both the G89 and Desaubies and Smith models assume a fixed relationship between *rms* shear and strain, it is impossible to determine whether strain should be the correct variable to track.

With the above caveats in mind, however, the apparent success of strain-based scaling of dissipation (assuming that the data sets analyzed by G89 all have canonical strain rates), suggests that dissipation rates can be estimated with some success from measurements of IW energy density and strain. A mooring with adequate vertical and temporal resolution of the density field might therefore be used to obtain dissipation rates on sufficiently large vertical and temporal scales, say 50 m and several days. These requirements would be most easily met by sufficiently rapid automatic yo-yo CTD devices with resolutions of about 1 m and a sampling rate greater than about 1 cycle/hour. The vertical span of the profile would need to encompass the upper and lower bounds of isopycnal excursions, which have *rms* vertical motions of $O(10)$ m in a GM ocean.

SUMMARY

Our studies of simultaneous measurements of IW properties and microscale dissipation rates in a region where many of the GM assumptions do not hold (although $E_{IW}/E_{GM} = O(1)$), leads us to the following conclusions.

(1) Large values of ϵ are found where the wave field is not well modeled by a Garrett-Munk spectrum, even where the energy density is comparable to the canonical values.

(2) Some modelling success might still be achievable in these regions, provided the vertical wavenumber bandwidth, β_*, can be estimated (perhaps from vertical and/or horizontal coherences in either the velocity or hydrographic fields). Automated yo-yo CTD profilers and a vertical current meter array appears to be the most likely technique for acquiring the required data from moorings.

We believe that it is still too early to claim even a "first-order" understanding of the processes by which energy is transferred through the IW spectrum to the dissipation scales. There is, however, some prospect that sufficiently robust empirical models can be developed to allow predictions of ϵ from long-term moorings, at least to within the accuracy obtainable by extrapolating the estimates from short-duration microstructure programs.

ACKNOWLEDGMENTS

We wish to express our appreciation for the efforts and hospitality of Peter Müller and Crystal Miles, who organized the 'Aha Huliko'a workshop. Discussions with several participants, notably Eric Kunze, Mike Gregg, and Greg Holloway, have been valuable to this study. This work has been sponsored by ONR, contracts N00014-87-K-0009 and N00014-90-J-1042 (LP, TM, HW, ML, CP), and N00014-90-J-1099 (RP).

REFERENCES

Baker, M.A. and C.H. Gibson, 1987: Sampling turbulence in the stratified ocean: statistical consequences of strong intermittency. *J. Phys. Oceanogr.*, **17**, 1817–1836.

Caldwell, D.R., T.M. Dillon and J.N. Moum, 1985: The Rapid Sampling Vertical Profiler. *J. Atmos. Oceanic Technol.*, **2**, 615–625.

D'Asaro, E.A., and J.H. Morison, 1991: Internal waves and mixing in the Arctic Ocean, *Deep-Sea Res.*, in press.

Desaubies, Y.J.F. and M.C. Gregg, 1981: Reversible and irreversible finestructure. *J. Phys. Oceanogr.*, **11**, 541–556.

Desaubies, Y., and W.K. Smith, 1982: Statistics of Richardson number and instability in oceanic internal waves. *J. Phys. Oceanogr.*, **12**, 1245–1259.

Gargett, A.E., P.J. Hendricks, T.B. Sanford, T.R. Osborn, and A.J. Williams III, 1981: A composite spectrum of vertical shear in the upper ocean. *J. Phys. Oceanogr.*, **11**, 1258–1271.

Gregg, M.C., 1989: Scaling turbulent dissipation in the thermocline. *J. Geophys. Res.*, **94**, 9686–9698.

Gregg, M.C., and T.B. Meagher, 1980: The dynamic response of glass rod thermistors. *J. Geophys. Res.*, **85**, 2779–2786.

Gregg, M.C., J.C. Shedvin, W.C. Hess and T.B. Meagher, 1982: Dynamic response calibration of the Neil Brown conductivity cell. *J. Phys. Oceanogr.*, **12**, 720–742.

Henyey, F.S., J. Wright, and S.M. Flatté, 1986: Energy and action flow through the internal wave field: an eikonal approach. *J. Geophys. Res.*, **91**, 8487,-8495.

Hunkins, K., 1986: Anomalous diurnal tidal currents on the Yermak Plateau. *J. Marine Res.*, **44**, 51–69.

Levine, M.D., 1990: Internal waves under Arctic ice pack during the Arctic Internal Wave Experiment: the coherence structure. *J. Geophys. Res.*, **95**, 7347,-7357.

McComas, C.H., and P. Müller, 1981: The dynamic balance of internal waves. *J. Phys. Oceanogr.*, **11**, 970–986.

McPhee, M.G., 1988: Analysis and prediction of short–term ice drift. *J. Offshore Mechanics and Arctic Engineering*, **110**, 94–100.

Osborn, T.R. and W.R. Crawford, 1980: An airfoil probe for measuring turbulent velocity fluctuations in water. In: *Air-Sea Interaction: Instruments and Methods*, Plenum Press, New York, 801 pp.

Padman, L., and T.M. Dillon, 1987: Vertical heat fluxes through the Beaufort sea thermohaline staircase, *J. Geophys. Res.*, **92**, 10799–10806.

Padman, L., and T.M. Dillon, 1991: Turbulent mixing near the Yermak Plateau during the Coordinated Eastern Arctic Experiment. *J. Geophys. Res.*, in press.

Wijesekera, H.W., L. Padman, T.M. Dillon, M.D. Levine, C.A. Paulson, and R. Pinkel, 1991: A comparison of internal wave dissipation models with CEAREX observations. (in preparation).

relative vorticity, $-|\zeta|$, to the planetary vorticity can result in the M_2 baroclinic tide becoming a free wave (*i.e.* $\omega > f - |\zeta/2|$). This effect is discussed in more detail in D'Asaro and Morison (1991). Perhaps more importantly, it becomes difficult or impossible to determine the free wave contribution from a near-inertial spectral peak, especially when measured from a non-stationary ice camp.

Fig. 7 shows frequency spectra for several relevant variables during the ice drift. These spectra are taken along an isopycnal with a mean depth near 150 m, near the ϵ peak, for the period $97.0 < t < 113.0$. The velocity spectrum is dominated by diurnal energy, with a secondary peak, as expected, near the inertial frequency. The cartesian coordinate shear spectrum shows that the diurnal tide is almost entirely barotropic, so that the near-inertial peak dominates. When the *magnitude* of the shear vector is analyzed (Fig. 7d) the dominant peak is again near-inertial, consistent with a shear vector that rotates with time rather than showing appreciable magnitude changes. Other spectra show the principal frequencies of variability in N, strain, and ϵ, and will be discussed further below. However, for the moment it is worth noting that the dominant time scales for variability of ϵ are diurnal and approximately 6 hours, the latter *not* corresponding to significant peaks in any of the obvious forcing functions.

With this degree of wave field variability in mind, we now consider higher order statistics of the displacement field, to see if there might be some obvious reason for the failure of the G89 model in this environment. One possible candidate is the effective vertical wavenumber bandwidth, β_*, which appears in the McComas and Müller (1981) and Henyey *et al* (1986) models (Eqs. 9 and 10, below). In practice, because β_* is expected to be a function of N, we consider instead the variability in the "equivalent number of vertical modes", $j_* = bN_o\beta_*/\pi N$, where N_o is a canonical buoyancy frequency ($0.0052\ \mathrm{s}^{-1}$), and b is the scale depth of the thermocline (1300 m). A typical mid-latitude value is $j_* = 3$.

Desaubies and Smith (1982) used an analytical approximation (Desaubies and Gregg, 1981) to the GM spectrum to show that shear variance was simply related to kinetic energy density by

$$\langle U_z^2 \rangle = \beta_* \beta_c \langle U^2 \rangle \tag{6}$$

where β_c is the cutoff wavenumber in the IW field, which Gargett *et al* (1981) suggested was constant at about $0.6\ \mathrm{m}^{-1}$. Desaubies and Smith argued that the statistics of mixing in a GM IW field are dependent only on the *rms* strain, λ_{rms}, where

$$\lambda_{rms}^2 = \langle (\partial\eta/\partial z)^2 \rangle \tag{7}$$

and η is an isopycnal displacement from its mean position. Desaubies and Smith speculated that the (at the time) apparent constancy of λ_{rms} in the open ocean